Scalability of Non-Intrusive Load Monitoring for Shipboard Applications

James Paris; Zachary Remscrim; LCDR Keith Douglas, USN; Dr. Steven B. Leeb; Dr. Robert W. Cox;
MKC Scott T. Galvin, USCG; MKC Steven G. Coe, USCG; LT Jennifer R. Haag, USCG;
LT J. Andrew Goshorn, USCG

Abstract—The non-intrusive load monitor has been demonstrated [1]–[3] as an effective tool for evaluating and monitoring shipboard electro-mechanical systems through analysis of electrical power data. A key advantage of the nonintrusive approach is the ability to reduce sensor count by monitoring collections of loads. This paper reviews tradeoffs that affect the likely performance of the NILM in a real world environment.
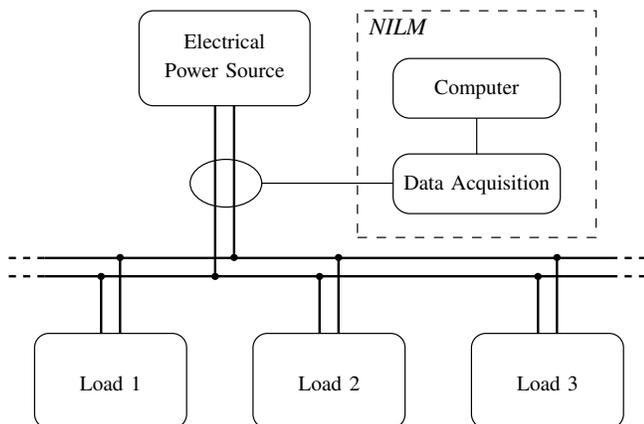
Fig. 1. Typical system layout for non-intrusive monitoring of several loads. Data acquisition and processing occurs at a central location.

Fig. 2. The USCGC ESCANABA (WMEC-907) in Boston, MA.

I. INTRODUCTION

The power distribution network can be pressed into "dual-use" service, providing not only power distribution but also a diagnostic monitoring capability based on observations of the way in which loads draw power from the distribution service. We have developed a nonintrusive power monitor for shipboard applications. Experiments with this monitor are reported in [2]–[12]. This power system diagnostic monitor uses existing power wiring to monitor loads. It is lightweight, cheap to install, and, because of its low sensor count, potentially highly reliable. References [13]–[19] demonstrate the NILM as a potentially effective tool for evaluating and monitoring shipboard mechanical systems through analysis of electrical power data. A key advantage of the nonintrusive approach is the ability to reduce sensor count by monitoring collections of loads.

The arrangement of the power wiring for these collections of loads determines the performance, accuracy, and usefulness of the NILM. This paper reviews tradeoffs that affect the likely performance of the NILM in a real world environment. In particular, these tradeoffs bound the size of the collection of loads that can be monitored, determining the extent of the "nonintrusiveness" that the monitoring system can deliver in practice.

Figure 1 shows a typical layout of the NILM, with one sensor monitoring three loads. Because the NILM can associate observed electrical waveforms with the operation of particular loads, it is possible to exploit modern state and parameter estimation algorithms to verify the operation and "health" of electromechanical loads [20], [21]. In order to minimize sensor count, a NILM installation would monitor as many loads as possible from a current sensor monitoring the aggregate feed to the loads.

Ideally, a single NILM could be used to measure and disaggregate all of the power usage of the electromechanical loads on a ship. However, there are practical limitations that prevent complete monitoring and individual tracking of each load as the total number of loads monitored on an aggregate feed increases. Specifically, there are at least three issues that could limit the extent to which a NILM can be "nonintrusive:"

- First, the NILM examines sampled or "quantized" observations of the measured current. This quantization is distributed over a finite range of observable currents, bounded by an absolute maximum current that can be measured by the combination of the sensor and associated analog-to-digital converter. Therefore, for a given hardware configuration, the dynamic power range of the NILM is bounded. As the NILM is pressed to monitor larger aggregate current feeds with bigger maximum currents, the smallest observable features or waveshapes become increasingly limited. Among other concerns, the
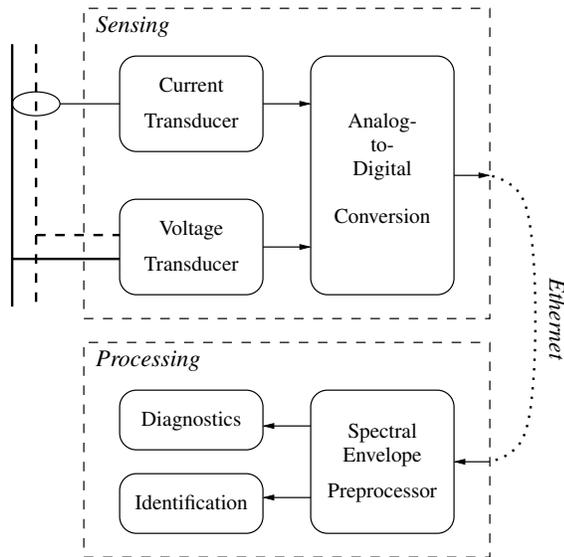
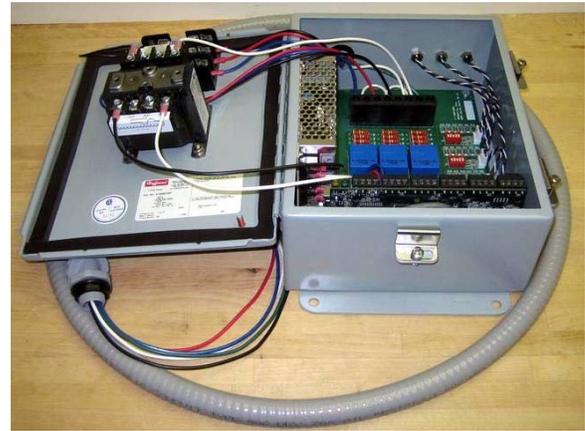Fig. 3. Data acquisition and processing flow in a NILM for AC loads

Fig. 4. NILM integrated sensor box, provided by Dr. John Rodriguez of NEMOmetrics, with integrated LabJack analog-to-digital conversion card. External connections are provided for power, current transducers, and Ethernet.

Fig. 5. NILM system as installed next to a power distribution panel on the USCGC ESCANABA. The NEMOmetrics sensor and data acquisition box, top, connects via Ethernet to a tablet PC, bottom.

power usage of small loads might barely register in the presence of much larger loads, due to limited resolution of the data acquisition.

- Second, the pickup of random noise or other distortions may increase as the NILM moves further away from monitored loads. Informally, the possibilities for pickup and coupling of electromagnetic noise may vary depending on the location where the NILM is installed.
- Third, some loads may be indistinguishable from each other or from the periodic variations of power demand associated with other or larger loads in the aggregate stream. For example, power demand oscillations associated with cyclically operated equipment like steering gear or fin stabilizers may fortuitously and unfortunately look like or mask the signals of other loads like motor pumps.

This paper examines all three of these issues to determine their likely effect on NILM performance, using analysis of the NILM techniques combined with real-world data and examples from the USCGC ESCANABA (Figure 2). This analysis could be used to determine the likely success of nonintrusive monitoring at any given point in a particular power system. It could also be used *a priori* to design a power system for shipboard applications that is intended to facilitate reliable nonintrusive monitoring.

II. THE NILM SYSTEM

Figure 3 shows a simplified diagram of the data acquisition and processing flow in a typical NILM installation for AC loads. In general, load monitoring is a three-step process consisting of:

1) Data acquisition, where electrical loads' current and voltage are measured and converted into digital form.
2) Preprocessing, where power usage or other useful attributes are extracted from the raw data.
3) Application-specific disaggregation, identification, and diagnostics.

The hardware that implements this process is designed to be modular and flexible. A custom integrated sensor box from NEMOmetrics, shown in Figure 4, provides a sealed enclosure that includes all data acquisition components with external connections for power, current transducers, and an electrically-isolated Ethernet data link. An embedded system or commercial off-the-shelf personal computer can be used to process, analyze, and store or report data on the monitored loads. Figure 5 shows a full NILM system as used on the USCGC ESCANABA. This installation utilizes a Thinkpad tablet PC to present a touchscreen user interface to the operator.

TABLE I
EXAMPLE CURRENT TRANSDUCERS AND CONVERSION RATIOS

Model	Maximum Primary Current	K_N
LA-55	± 50 A	1/1000
LA-150	± 150 A	1/2000
LA-205	± 200 A	1/2000
LA-305	± 300 A	1/2500

TABLE II
EXAMPLE ANALOG-TO-DIGITAL CONVERTER SPECIFICATIONS

| Model	Voltage Range (V_R)	Output Range	Bits (B)
PCI-1710	± 10 V (selectable)	$0 \rightarrow 4095$	12
LabJack	± 5 V	$0 \rightarrow 65520^1$	12
NerdJack	± 10 V (selectable)	$0 \rightarrow 65535$	16

Fig. 6. Quantization error, as would be introduced by a linear ADC. The continuous function $\sin(x)$ is compared to the same function represented discretely with only 4 and 2 bits of resolution.

The NILM processing workflow for AC loads is examined below, with particular emphasis on details relevant to sensor reduction and scalability.

A. Data Acquisition

Data acquisition measures the voltage and current supplied to a load or collection of loads, converting these observations into digital form at the computer. Voltage and current are measured similarly, but this discussion will focus on the current for simplicity. The current carries the majority of information used by subsequent processing steps.

Current is measured using a current transducer (CT). This active device is placed around a current-carrying wire going to a particular collection of loads, also known as the primary current I_P. The CT provides an output pin where a scaled copy of the measured current is produced as the secondary current I_S. The ratio of primary current to secondary current is the conversion ratio, denoted K_N. Typical CTs used for NILM are shown in Table I.

The secondary output I_S of a CT is then placed across a burden resistor R_M to ground. The measured voltage V_M across this resistor is proportional to the primary current I_P by the relation

$$V_M = I_S \times R_M = I_P \times K_N \times R_M \qquad (1)$$

For example, the measured voltage range V_M for a LA-55 at maximum current with a 50 Ω burden resistor would be

$$V_M = \pm 50 \text{ A} \times \frac{1}{1000} \times 50 \ \Omega \qquad (2)$$

$$= \pm 2.50 \text{ V} \qquad (3)$$

An analog-to-digital conversion (ADC) card connected to a computer is used to sample the voltage V_M at a rate of 8000 samples per second. This introduces quantization error, because the digital result of the sampling has a fixed limited resolution as determined by the characteristics of the ADC. The ADC resolution is typically expressed as the number of significant binary bits B used to represent the digital result. B binary bits can represent a total of 2^B discrete values, and these 2^B values correspond to equally-spaced discrete voltages across an ADC card's specified input voltage range. Voltages that fall in-between are rounded to the nearest discrete value, and this rounding or truncation is the source of the quantization error. Figure 6 demonstrates the quantization of a sine wave at two levels, $B = 4$ bits and $B = 2$ bits, which correspond to 16 and 4 discrete levels, respectively.

---

[1]The LabJack software outputs 16-bit values, but only the top 12 bits of the output value are significant. The low-order 4 bits are always read as 0.
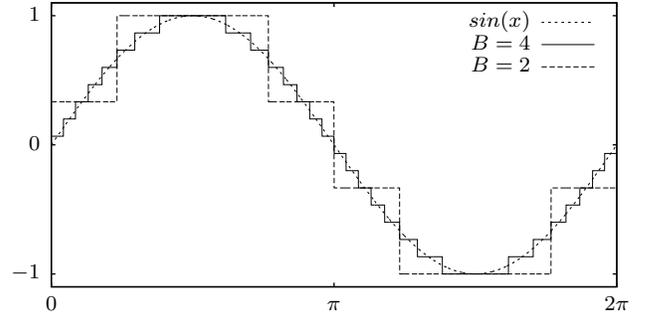
The choice of ADC card for the NILM has evolved over time to the meet the needs of aggregate load monitoring. Specifications for some relevant cards are shown in Table II. Many of our early shipboard NILM systems were deployed using the Advantec PCI-1710, a PCI add-in card compatible with standard desktop computers, that provides accurate and reliable measurement while supporting the NILM's required 8 KHz data rate. The primary drawback of the PCI-1710, however, is that laptops, tablet PCs, and embedded systems cannot easily integrate a PCI card. This limits installation flexibility, as a NILM utilizing this card can only be placed in a location within several feet of a desktop computer.

To provide flexibility to a system designer integrating the NILM, recent installations have been developed using the LabJack UE9 Ethernet-based acquisition card. An electrically-isolated data interface with maximum lengths of at least 100 meters, Ethernet provides significant benefits in that it allows the acquisition and data processing to occur at physically disjoint locations, making installations such as the one shown in Figure 5 possible.

Recently, MIT has developed a new custom Ethernet-based ADC card to further improve NILM data acquisition. The NerdJack, shown in Figure 7 and described in [22], improves on the LabJack by increasing the supported voltage range and number of bits B from 12 to 16, which reduces the ADC quantization error. This will allow the NILM to accurately resolve smaller currents, improving performance as larger collections of loads are monitored and reducing the accuracy error detailed in Section III-A. Other features include LabJack form-factor compatibility, faster sampling rates, more input channels, and hardware expandability for future data pre-processing frontends. The NerdJack is undergoing final testing and is expected to begin replacing the LabJack in new NILM installations within the next few months.

The accuracy of the chosen ADC card can be related to the voltage V_M as follows. The values in Table II give, for each
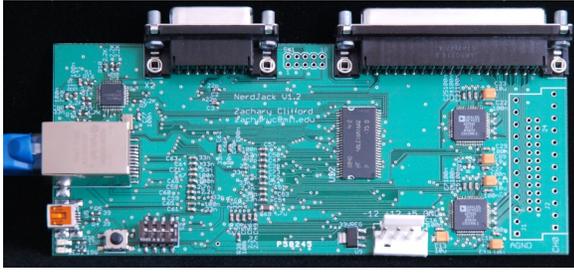
Fig. 7. The custom "NerdJack" Ethernet-based data acquisition card, currently under development by Zachary Clifford at MIT [22].

(a) Raw current and voltage.

(b) Spectral envelope output from the preprocessor.

Fig. 8. Motor start transient as measured by the NILM.

ADC card, the specified maximum input voltage range V_R, and the number of significant bits B. As these bits are evenly distributed over the integer codes, the absolute accuracy can be computed in terms of measured voltage per least-significant-bit (LSB) as

$$V_{M,\text{LSB}} = |V_R|/2^B \tag{4}$$

For the LabJack, where $V_R = \pm 5$ V and $B = 12$,

$$V_{M,\text{LSB}} = \frac{((+5 \text{ V}) - (-5 \text{ V}))}{2^{12}} \tag{5}$$

$$\approx 2.441 \text{ mV} \tag{6}$$

This is the maximum accuracy. Note that it covers the entire ± 5 V range of the ADC, while Equation 3 shows that the measured voltage V_M will only reach ± 2.50 V. This inefficiency leads to a loss of resolution, and can be mitigated somewhat by different choice of CT, burden resistor, and ADC, when possible.

The maximum accuracy can then be converted to equivalent primary current per LSB using Equation 1, which for our model CT configuration gives

$$I_{P,\text{LSB}} = \frac{V_{M,\text{LSB}}}{K_N \times R_M} \tag{7}$$

$$= \frac{2.441 \text{ mV}}{1/1000 \times 50 \text{ }\Omega} \tag{8}$$

$$\approx 48.82 \text{ mA} \tag{9}$$

Another useful metric is the effective number of bits corresponding to a particular size load being measured. To find this, the number of LSBs N corresponding to the amplitude I of the load can be computed from Equation 7 as
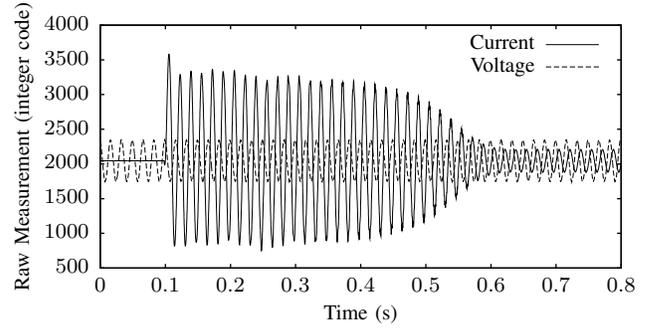
$$N = I/I_{P,\text{LSB}} \tag{10}$$

From this, the effective number of bits B_E is

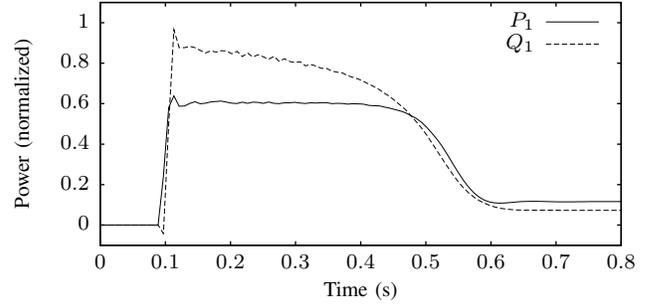$$B_E = \log_2(N) = \log_2(I/I_{P,\text{LSB}}) \tag{11}$$

As an example, a ± 5 A load being measured by the model setup is effectively being measured with a resolution of

$$B_E = \log_2\left(((+5 \text{ A}) - (-5 \text{ A}))/48.82 \text{ mA}\right) \tag{12}$$

$$\approx 7.68 \text{ bits} \tag{13}$$

For ease of calculation, Equation 11 can be expanded to give the complete formula for effective number of bits

$$B_E = \log_2\left(\frac{I \times K_N \times R_M \times 2^B}{|V_R|}\right) \tag{14}$$

where, as before,

$$I = \text{amplitude of load current}$$
$$K_N = \text{CT conversion ratio}$$
$$R_M = \text{CT burden resistor}$$
$$|V_R| = \text{amplitude of ADC voltage input range}$$
$$B = \text{ADC rated number of bits at full range}$$

For illustration in the next sections, Figure 8a demonstrates the raw voltage and current waveforms acquired by the NILM during an electric motor startup. The raw measurement integer code corresponding to zero input signal is determined by the ADC specifications, and is 2048 in this example.

B. Spectral Envelope Preprocessor

The NILM employs a preprocessing step to extract spectral power envelopes from the raw voltage and current waveforms. Existing research has demonstrated the utility of this preprocessing step for identifying transient electrical signatures in a wide variety of applications [1], [3], [20], [23]–[26]. Preprocessing exposes energy consumption and harmonic signatures that are relatively uniquely associated with the physical task performed by a load. Preprocessing raw data eliminates distracting data artifacts, such as the underlying 60 Hz carrier wave of an AC power system, and reveals fingerprint signatures that can be used to identify load operation and diagnostic conditions.

The spectral envelopes extracted by the preprocessor are are short-term averages of harmonic content present at each of the harmonics of the incoming line frequency. As reviewed in [23], the in-phase spectral envelopes a_k of an input current signal $x(t)$ are

$$a_k(t) = \frac{2}{T} \int_{t-T}^{t} x(\tau) \sin(k\omega\tau) d\tau \qquad (15)$$

where k is the harmonic index, and the quadrature spectral envelopes are

$$b_k(t) = \frac{2}{T} \int_{t-T}^{t} x(\tau) \cos(k\omega\tau) d\tau \qquad (16)$$

For NILM applications, the time t is referenced such that the term $\sin(\omega\tau)$ in Equation 15 is phase-locked to the voltage measurement, which can be achieved using a Kalman filter [27] to determine voltage-waveform zero-crossings. The averaging interval T is one or more periods of the line frequency. Under these conditions, the spectral envelopes are computed as $P_k = a_k$ and $Q_k = -b_k$, and these are the outputs of the preprocessor. The outputs are defined in this way so that the values P_1 and Q_1 correspond to the conventional definitions of real and reactive power.

Originally a choice for highlighting recognition features, the NILM preprocessor also has useful ramifications regarding signal quality in the presence of quantization and noise. These benefits are examined more closely in Section III-B.

The first two spectral envelope harmonics corresponding to a motor start, as computed by the NILM preprocessor, are shown in Figure 8b.

C. Load Identification and Diagnostics

The NILM uses the spectral preprocessor output to perform load disaggregation, to identify the operating schedules of specific loads, and to extract diagnostic information and other application-specific indicators about the loads. A useful method for extracting these identifying features relies on the power transients, which are associated with any event in which the power usage of the system changes quickly. Typically, this occurs when a load turns on and off, and may also occur during cyclical operation. Transient power changes may also occur in the event of failures such as the physical breaking of a link or the failure of a reverse-osmosis membrane. Transients are useful for diagnostic estimation because, for electro-mechanical systems, the transients may be rich in frequency content and amplitude.

Matching transient power signatures relies on finding unique aspects of a load's power usage. In many simple cases, matching shape of the transient is sufficient, and the transients can be identified by comparing against exemplars, as demonstrated in Figure 9. When scaling to larger NILM installations that incorporate many loads, more complex methods of identifying transients may be required, as discussed in section V.

III. Measurement Accuracy

Sensor count and installation complexity are reduced with the nonintrusive approach by placing the measurement system
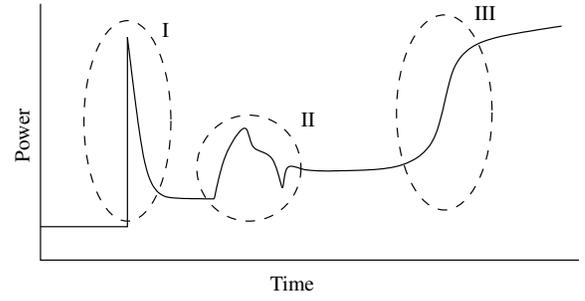

Fig. 9. Startup power usage of a single device, with three component power transients identified through exemplar matching. From [24].
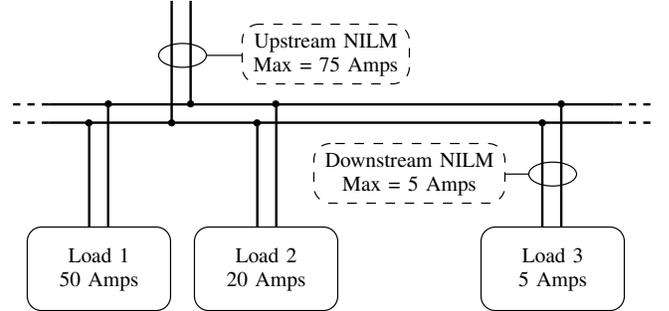

Fig. 10. Two potential locations for a NILM installation. The "upstream" NILM monitors all three loads, while the "downstream" NILM monitors only one load.

at a location that encompasses multiple loads. To reliably identify load operation and diagnose load problems, the NILM must disaggregate the power usage and harmonic content of individual load transients with some level of accuracy. A useful procedure for evaluating the NILM's ability to disaggregate loads is to examine the identification performance as the number of monitored loads is increased.

For discussion, consider the installation of an "upstream" and "downstream" NILM for comparison, as shown in Figure 10. The upstream NILM will see the net power usage of all three loads, up to a steady-state maximum of 75 A, whereas the downstream NILM is only monitoring a single load with a maximum steady-state current of 5 A.

A. Accuracy of Raw Data

One limitation pertaining to the upstream NILM's performance relative to the downstream system is that the current transducers and analog-to-digital conversion systems have a fixed accuracy. To meet the upstream and downstream load requirements in Figure 10, a system designer might consider Tables I, II and other requirements to decide on the following configurations:

	Upstream	Downstream
Transducer	LA-205	LA-55
Conversion Ratio	$K_N = 1/2000$	$K_N = 1/1000$
Burden Resistor	$R_M = 5 \ \Omega$	$R_M = 155 \ \Omega$
Voltage Range	$V_R = \pm 5$ V	$V_R = \pm 5$ V
Bits	$B = 12$	$B = 12$

Now consider the power usage of a single load measured by both systems, Load 3. Assume that this load has a startup
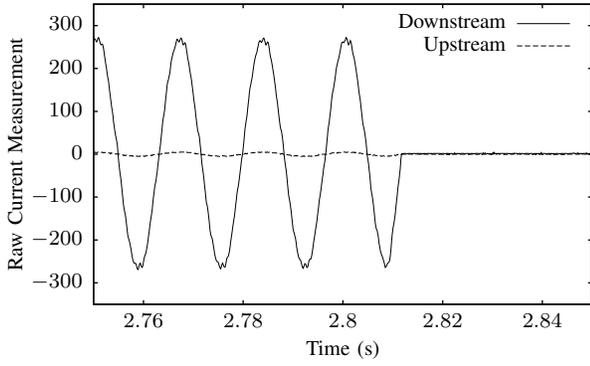
(a) Raw data from both configurations on the same scale.
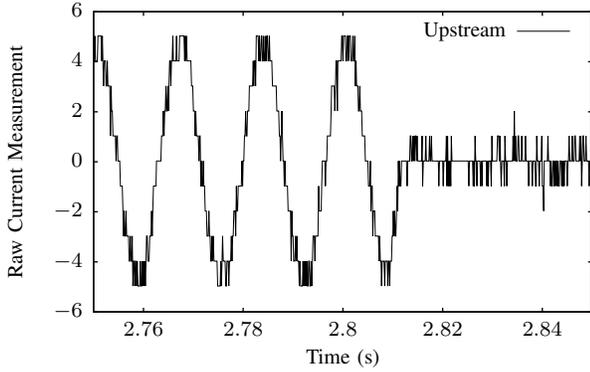
(b) Raw upstream data, enlarged to show detail.

Fig. 11. Two NILM configurations recording the same transient event. The upstream configuration is scaled to handle much larger loads, but cannot resolve the finer details of a single load due to quantization.

power transient with amplitude $I = 5$ A that each NILM is capturing through the data acquisition process described in Section II-A. Equation 14 can be used to compute the effective number of bits $B_{E,D}$ of the raw current measurement for the downstream setup as

$$B_{E,D} = \log_2 \left(\frac{5 \times 1/1000 \times 155 \times 2^{12}}{10} \right) \quad (17)$$

$$\approx 8.31 \text{ bits} \quad (18)$$

and similarly compute $B_{E,U}$ for the upstream setup

$$B_{E,U} = \log_2 \left(\frac{5 \times 1/2000 \times 5 \times 2^{12}}{10} \right) \quad (19)$$

$$\approx 2.36 \text{ bits} \quad (20)$$

This loss of nearly 6 bits of accuracy represents a significant degradation in resolving the raw current due to measurement scaling and quantization during the analog-to-digital conversion process.

To demonstrate the practical implications of this effect, experiments were performed in February 2009 on the USCGC ESCANABA (Boston, MA). A single run of the collection-hold-transfer (CHT) vacuum pump was captured simultaneously by upstream and downstream NILM systems in the described configurations, with no additional loads active at the time. A portion of the pump's transient at shutoff is shown in

Figure 11. As calculated, the upstream data shows significantly less resolution and accuracy compared to the downstream data. In the detailed view of Figure 11b, smaller changes in the raw current are indistinguishable from the quantization noise due to the reduced accuracy.

In general, the accuracy of the raw current data acquisition for any particular load will linearly decrease as the maximum load capacity of the NILM increases, given that the ADC parameters are fixed. For example, if the NILM is sized to handle twice as much aggregate current, then the power usage of any individual load will be measured with half the resolution. As the NILM scales to more loads, the raw resolution may be severely reduced.

B. Accuracy of Spectral Envelopes

Fortunately, most existing NILM analysis techniques do not make direct use of raw current data, relying instead on the pre-processed spectral envelope output. In most applications, the usage is more specifically limited to only the first harmonics of in-phase and quadrature power, P_1 and Q_1. The full effect of measurement quantization in these common cases therefore depends on how the raw error affects the calculation of these values.

As shown in Equations 15 and 16, P_1 and Q_1 correspond to averages over a single 60 Hz period of the incoming voltage and current waveforms. Informally, this has a "smoothing" effect on the data similar to applying a low-pass filter, and high-frequency deviations will be averaged out by the pre-processor. Quantization error in the raw data will then have a limited impact, as long as the mean value still approaches the actual power usage of the load. In effect, the preprocessor uses the high-speed, quantized sampled data from the data acquisition to produce good quality output at a lower rate.

Figure 12 demonstrates this effect of the preprocessor on the two NILM configurations tested on the USCGC ESCANABA. Although the upstream quantization error in Figure 11b is readily apparent, the preprocessor's spectral envelope output for downstream and upstream data in Figures 12a and 12b are very similar. Both show fine details of the pump's power usage, particularly during the startup transient. Figure 12c demonstrates this accuracy by plotting the error as a percentage of the full amplitude of the transient; the error is generally within $\pm 1\%$ for the duration of the pump run.

This result demonstrates that moving the NILM upstream does not cause significant loss of accuracy due to quantization and measurement error, in the common case that spectral envelopes are the metric used for identification and diagnostics. A more formal analysis of the effects of quantization error on the output of the preprocessor will be published in [28]. Preliminary results indicate that, given reasonable assumptions about the nature of the quantization process and the power usage of real-world loads, the effects of quantization alone are minimal, and are expected to be comparable or better than the results demonstrated here on the USCGC ESCANABA.
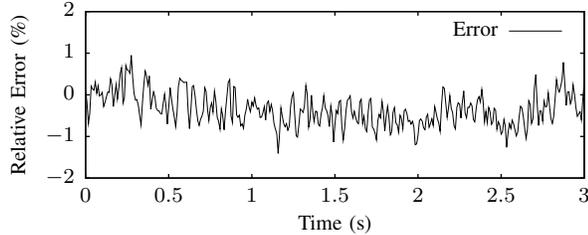
IV. MEASUREMENT DISTORTION

Noise comes in many forms. For load monitoring purposes, signal and measurement distortion generally refers to an exter-
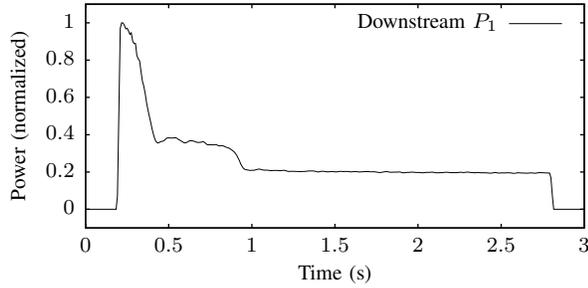
(a) Spectral envelope of the downstream measurement.
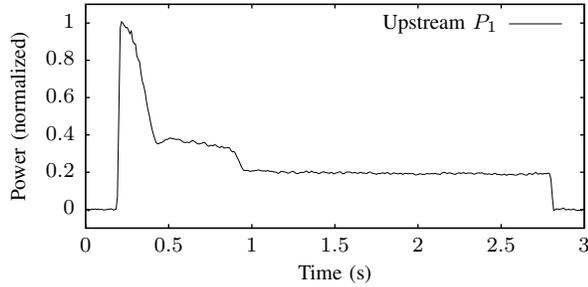
(b) Spectral envelope of the upstream measurement.

(c) Difference, as a percentage of the full transient amplitude

Fig. 12. Comparison of preprocessor spectral envelope output for the raw waveforms from Figure 11.

nal and undesirable corruption of the voltage and current waveforms as measured by the NILM data acquisition. Depending on the nature of the distortion, it can also be carried through NILM processing steps and indirectly affect identification and diagnostics. There are many potential means by which noise or other distortions can be introduced to the power distribution and monitoring system, including electromagnetic pickup by the wiring network, thermal noise in electronic components, and magnetic interference at the sensor.

A. Uncorrelated Noise

The robust design of the NILM preprocessor allows it to reject many uncorrelated sources of noise, where the additive effect of the noise is independent of the input waveforms. One such type of noise is additive white Gaussian noise (AWGN). This type of noise is normally-distributed around zero and uncorrelated, and might be expected to appear as a result of thermal noise in the system. It can be shown [28] that the energy of this noise is equally distributed across all frequencies.

The spectral envelope calculation is particularly well-suited to handle such noise. For example, the NILM preprocessor

utilizes a Kalman filter or phase-locked loop to reduce error in the detected voltage zero-crossing points. This filter has a high noise rejection capability, as examined in [27], and so the NILM is largely unaffected by noise on the voltage input.

For the current measurement, the effect of white noise at the preprocessor is closely related to the effect of quantization noise in the acquisition process, as described in Section III-B. The spectral envelope calculation involves extracting harmonic content at specific frequencies that are low multiples of the 60 Hz line frequency. Since white noise is equally distributed across all frequencies, the contribution of such noise to any particular harmonic power envelope is small.

Furthermore, the presence of uncorrelated noise appears minimal in practice. In Figure 11b, which shows the high level of quantization when the NILM is scaled to handle upstream loads, the visible noise in the waveform is still within $\pm\frac{1}{2}$ LSB, which is the accuracy rating of the analog-to-digital converter itself. It is therefore expected that this type of noise will not be a significant limiting factor for NILM scalability.

B. Correlated Noise and Coupled Signals

Some sources of signal distortion may be related to the original signal itself or might be caused by other external factors that are not distinguishable from the correct data. One potentially large source is electromagnetic coupling and pickup between any electric circuits or loads. Changing currents in a motor, transformer, or just the power distribution wiring will generate magnetic fields which can induce related currents in other systems. From the measurements performed by the NILM, these distortions may be perceived as additional loads, or they may negatively affect sensitive diagnostics of existing loads.

Increasing the number of loads monitored by the NILM will generally exacerbate the problem, as additional loads utilize additional wiring and components that can both radiate or couple and receive the noise. Unlike uncorrelated noise, which the preprocessor is already capable of rejecting, this type of noise is not easily rejected and any increases are undesirable. While the net effect has been low in observed systems, distortion coupling can potentially be complex and relate closely to specific installation details, so it is important to consider these effects.

Fortunately, there are several mitigating factors and techniques that can be used to reduce the impact of signal coupling and correlated noise. For example, many circuits and distribution panels are already in shielded and isolated metal enclosures, like the NEMOmetrics NILM sensor box in Figure 4; while nominally done for safety purposes, this is also an effective and simple way to isolate a circuit from electromagnetic interference.

For situations where a ship-board power system is designed a priori to facilitate nonintrusive monitoring, the system designer may be able to manage noise coupling between individual loads to place susceptible loads further apart, or even choose loads that are known not to interfere with each other. For wiring runs between distribution panels and loads, coupling can be reduced by physically separating wires or by

utilizing separate conduit for separate feeds. Wiring layout to enhance monitoring might become as important a concern as wiring for redundancy and combat survivability, as effective monitoring can enhance operational readiness.

The choice of location for the NILM monitoring hardware can also have an effect on noise pickup. For instance, consider a generator with a long distribution wire running to a room of loads. A NILM intended to monitor these loads would likely see less noise pickup if placed at the entrance to the room rather than at the generator. The modular design of the NILM shown in Section II is explicitly intended to support this type of installation, and features like the Ethernet connection allow the data acquisition and processing hardware to be physically separated with no loss of quality or performance.

Finally, as the size of the set of monitored loads increases, the NILM has more information about the state of the power system, and in particular the operating schedule of specific loads. This information may be useful in reversing the effects of coupled noise. For example, if the system designer determines that running Pump A causes excessive noise to be picked up by Pump B, the load monitor could potentially be improved to correct for and remove this additional noise whenever Pump A is running. However, this and other advanced techniques have not been necessary in practice; coupled noise does not appear to be a significant problem in current installations.

V. Disaggregation

The ability to distinguish or disaggregate load transient shapes from the background variations created by other loads is the third and potentially most complex issue affecting the scalability of the non-intrusive load monitor. Of course, the ability of the NILM to operate given only an aggregate power measurement leads to sensor reduction and installation flexibility. However, larger and more challenging or variable collections of loads may limit the NILM's ability to decompose a combined measurement into individual operating waveforms. Some of the details of the signal processing approach to disaggregation are necessarily site or application specific. For example, when measuring the combined power usage of a collection of electric motors, one application may require simply knowing how many motors are on, while another might require the ability to determine operating schedules for each specific motor individually. The NILM's utility and precise placement will vary in these two scenarios.

A. Methods of Disaggregation

The basic requirement for successful disaggregation is that there exist some unique metric or feature of an individual system's power usage that distinguishes between the loads of interest. Typical metrics include steady-state power levels and transient shape, amplitude, and sequencing. More advanced metrics include frequency domain analysis and the use of the higher-order harmonic spectral envelope data from the preprocessor. In some cases, these metrics may not be fully known or repeatably characterizable, but can be distinguished using machine learning algorithms that perform feature-based clustering either automatically or based on supplied training data.

Experience has shown that transient analysis is a particularly useful technique for identification and diagnostic monitoring [5], [7]. As the NILM scales to monitoring larger collections of loads, two issues in particular can make transient analysis difficult. First, transients associated with distinct physical events may overlap, and adding more loads to the system may increase the chance of this occurring. Second, classification of a transient generally requires that the steady-state power usage of the system is otherwise quiescent so that the shape can still be correctly recognized. As the number or size of loads in the system increase, small-scale variations in steady-state power usage may combine to form larger variations and mask the transients of interest.

There are a number of potential solutions to the overlap issue. Sometimes, the chance of transient overlap may simply be acceptably low, given a load's expected operating schedule and transient width. In other cases, the distinct physical events may be related, as with a fan that always turns on shortly after a heater. For this situation, the combination of two transients might be trained as a single event for purposes of classification. Alternately, if the system can correctly identify the first transient, the classifier could subtract its known shape from the remaining data, effectively removing its influence when classifying the subsequent transient.

Similar techniques can be used to manage predictable steady-state variations. An unbalanced motor or a motor driving an eccentric or side-loaded mechanism, for instance, might wobble and show periodic variations that can be measured and subtracted. In many cases, however, the cumulative effect of the steady-state variations of aggregate power load can be complex and may even resemble non-deterministic signal noise. In these cases, statistical approaches can be applied to remove undesired features. Low-pass and other frequency-based filters can remove periodic variations. The median filter is particularly useful at cleaning up a steady state signal because it can preserve sharp edges, which may be useful for transient identification.
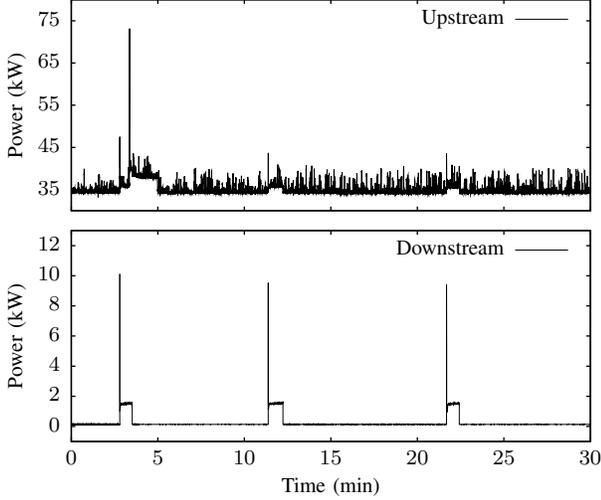
B. Experimental Data

To demonstrate the capability of the NILM to disaggregate loads, two monitoring systems were installed on the USCGC ESCANABA in September 2008. Several weeks of data were collected from "upstream" and "downstream" power feeds as in Section III. The downstream NILM monitored the collection-hold-transfer (CHT) pumps, and the upstream NILM monitored these plus many other larger loads, including the reverse-osmosis (RO) system and fin stabilizers. The sensor configuration is shown in Table III.

The effective number of bits (Equation 14) for a 10 A load as measured upstream and downstream are $B_{E,U} = 6.8$ and $B_{E,D} = 7.8$, respectively; this difference is small enough that there is not significant quantization in the upstream data.
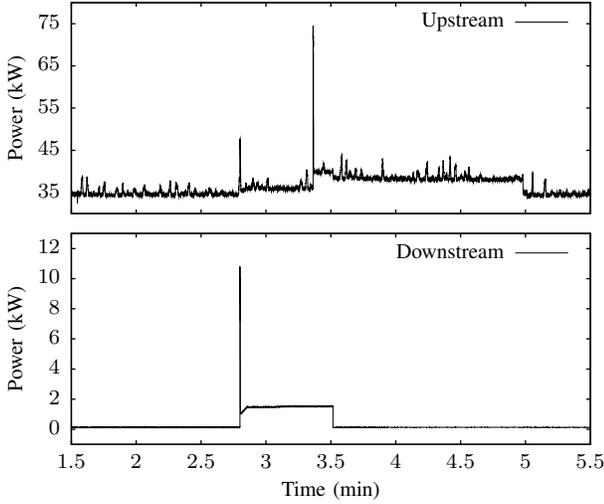
This experiment sought to determine if the relatively small CHT pump runs could be reliably identified in the upstream data. Figure 13a shows a representative sample of P_1 spectral

(a) Full window with three CHT pump runs. The upstream power usage includes additional transients and noise on top of a steady 35 kW load.

(b) Closeup of the first CHT pump run, with a larger unrelated transient captured by the upstream NILM.
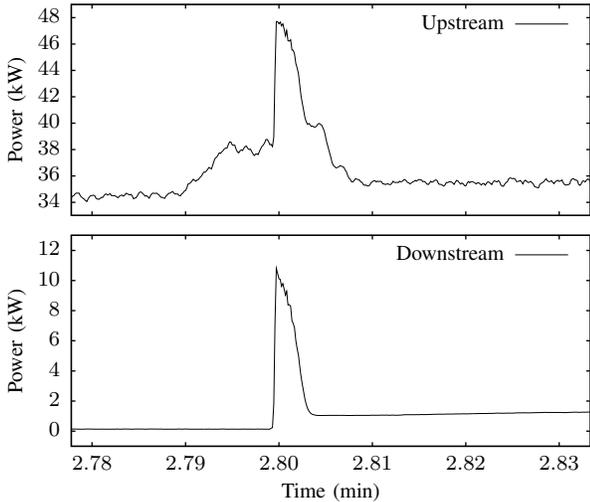
(c) Detail of the startup transient of the CHT pump. The general shape is still present in the upstream data.

Fig. 13. Three comparisons of the time-aligned P_1 spectral envelopes captured by the upstream and downstream load monitors.

TABLE III
SENSOR CONFIGURATION FOR DISAGGREGATION EXPERIMENT

	Upstream	Downstream
Transducer	LA-205	LA-150
Conversion Ratio	$K_N = 1/2000$	$K_N = 1/2000$
Burden Resistor	$R_M = 50\ \Omega$	$R_M = 100\ \Omega$

envelope data captured on October 22, 2008 from 0430-0500. The downstream power shows three CHT pump runs and no other loads. The upstream power, conversely, shows a significant continuous steady-state load of 35 kW as well as numerous other transients. Figure 13b shows a detailed view of the first CHT pump run. Note how the upstream NILM captured a larger unrelated transient that occurred during the CHT pump run, and the large amplitude of steady-state variations relative to the size of the downstream data. These issues can prevent proper classification [12].

However, classification is still possible. As shown in Figure 13c, the general shape and amplitude of the pump's initial power transient is retained and visible at the upstream NILM. Assuming this shape is unique, locating it in the upstream power data will reveal the times at which the CHT pump started.

C. Matching Waveforms

After removing DC offset, one common measure of similarity between two sampled waveforms $f[n]$ and $g[n]$ of equal size N is the Euclidean distance, defined as

$$D = \sum_{n \in N} (f[n] - g[n])^2 \tag{21}$$

This expression can be expanded as

$$D = \sum \left((f[n])^2 - 2f[n]g[n] + (g[n])^2 \right) \tag{22}$$

$$= \sum f[n]^2 + \sum g[n]^2 - 2 \sum f[n]g[n] \tag{23}$$

Expressed as a dot product, this is

$$D = (f \cdot f) + (g \cdot g) - 2(f \cdot g) \tag{24}$$

$$= |f|^2 + |g|^2 - 2(f \cdot g) \tag{25}$$

If the waveforms match, the Euclidean distance between them would be $D = 0$, and this equation reduces to

$$0 = |f|^2 + |g|^2 - 2(f \cdot g) \tag{26}$$

$$f \cdot g = \frac{|f|^2 + |g|^2}{2} \tag{27}$$

Furthermore, if the amplitudes match, $|f| = |g|$, so

$$f \cdot g = \frac{2|g|^2}{2} \tag{28}$$

$$\frac{f \cdot g}{|g|^2} = 1 \tag{29}$$

If Equation 29 holds, then the two waveforms match. Therefore, given f as our input signal and g as an exemplar, or example waveform, that we wish to find, $M = (f \cdot g)/|g|^2$
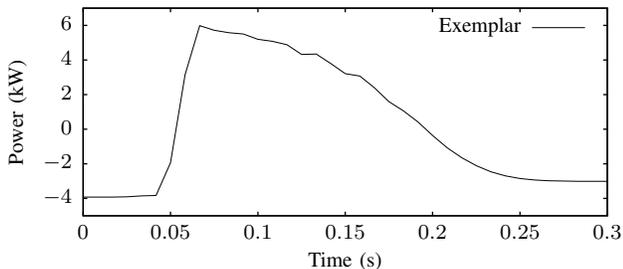
Fig. 14. Exemplar used to match the CHT pump startup transient.

is a useful figure of merit. As this value approaches 1.0, we can be reasonably confident that f and g match both in shape and amplitude. Requiring that the amplitude also match is an important restriction when dealing with aggregate data that incorporates many differently-sized loads that may share a similar shape.

When the full waveform f contains more points than the exemplar g, we can iterate or "slide" the exemplar across the data, computing the metric M at each point based on the inner product of a windowed subset of f and g. As the exemplar g approaches a feature in the data f that matches in shape and amplitude, the value of the figure of merit M will approach a local maximum of 1.0.

A significantly faster method of computing the same metric is based on cross-correlation [29]. Briefly, for two waveforms x and y, the cross-correlation is defined as:

$$(x \star y)[n] = \sum_{m=-\infty}^{\infty} x^*[m]\, y[n+m] \qquad (30)$$

where x^* denotes the complex conjugate of x. For real numbers, this represents the same basic operation as the dot product $(x \cdot y)$. Cross-correlation can be computed using the discrete Fourier transform $\mathcal{F}$ using the relation

$$\mathcal{F}\{x \star y\} = \mathcal{F}^*\{x\}\mathcal{F}\{y\} \qquad (31)$$

We are currently evaluating the use of such spectral methods for transient identification. Preliminary testing indicates that this technique can speed up the analysis of the data by several orders of magnitude.

D. Application and Results

To locate CHT pump startup transients in the upstream data, one sample exemplar of the transient was extracted from the downstream CHT data, and DC offset was removed, as shown in Figure 14.

Then, the correlation was computed between this exemplar and the full window of data from Figure 13a. Figures 15a and 15b present closeups of the correlation results for downstream and upstream data, respectively, at a time when the CHT pump turned on. As expected, the correlation approaches 1.0 as the time nears the pump start. A peak-detection algorithm with a small detection window between 0.9 and 1.1 is used to identify these points automatically.
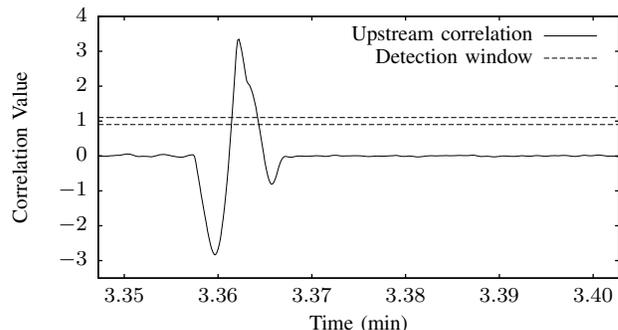
An example of the behavior of the event detector when confronted with an event that is different from the exemplar is
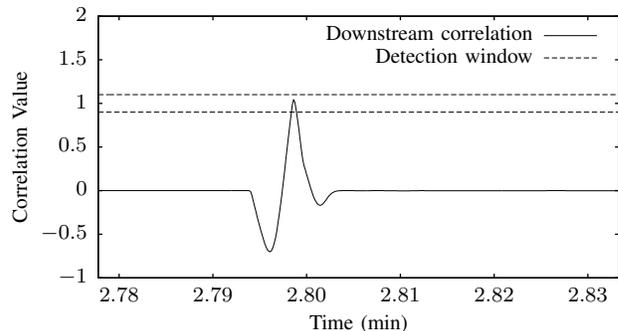
(a) Exemplar match against a CHT pump startup recorded downstream.
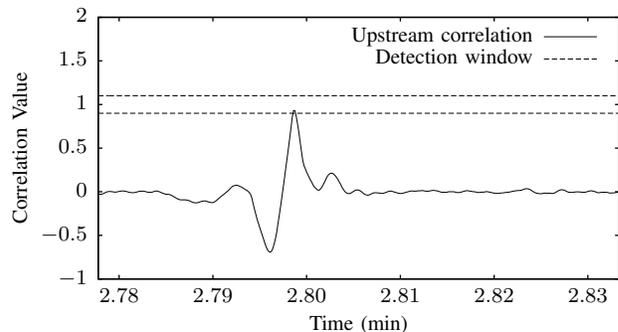
(b) Exemplar match against a CHT pump startup recorded upstream.

(c) Exemplar mis-match against a non-CHT transient recorded upstream.

Fig. 15. Calculated correlation value (figure of merit) between the exemplar and measured spectral envelopes. Local maxima near $y = 1.0$ indicate a strong correlation at time t.

shown in Figure 15c. In this case, the exemplar is compared to a large transient that is similar in shape to the CHT pump startup transient. However, this event is created by another device and is larger in magnitude than the CHT transient. The computed correlation value does cross through the detection window around 1.0, but the local maximum far exceeds the window and so this transient is correctly not identified as a CHT pump.

This technique is effective at finding the startup transient. In the downstream and upstream data, it detects three pump starts, at 2.80 minutes, 11.38 minutes, and 21.69 minutes. Further tests were run on similar data corresponding to 21 disjoint hours over the three-week period from October 10 to October 20. For every CHT pump transient found in the clean downstream data, the same event was correctly detected at the same time in the upstream data, with no false positives or

negatives, demonstrating that disaggregation can be performed reliably and quickly even in the presence of large unrelated variations and transients in the aggregate data.

VI. Conclusion

At least three issues make it challenging to extent a non-intrusive load monitor to monitor an increasing variety and number of loads: quantization, measurement noise, and the ability to disaggregate loads. The design of the NILM has been shown in this paper to effectively mitigate both quantization and measurement noise through the use of the spectral envelope preprocessor, as experimental data from the USCGC ESCANABA indicates. Neither of these factors is likely to be a significant concern as the NILM scales to monitor larger systems.

Effective disaggregation of load characteristics can be very application-specific, and may therefore require application-specific analysis. Nevertheless, several techniques were presented to improve disaggregation of loads in general cases, and many of these techniques can be applied to systems of all sizes. As shown on the USCGC ESCANABA, cross-correlation and exemplar matching can be used to identify transients quickly and accurately in real-world aggregate data.

References

[1] J. S. Ramsey, S. B. Leeb, T. DeNucci, J. Paris, M. Obar, R. Cox, C. Laughman, and T. J. McCoy, "Shipboard applications of non-intrusive load monitoring," in *American Society of Naval Engineers Reconfigurability and Survivability Symposium*, Atlantic Beach, Florida, February 2005.

[2] T. DeNucci, R. Cox, S. B. Leeb, J. Paris, T. J. McCoy, C. Laughman, and W. Greene, "Diagnostic indicators for shipboard systems using non-intrusive load monitoring," in *IEEE Electric Ship Technologies Symposium*, Philadelphia, Pennsylvania, July 2005.

[3] W. Greene, J. S. Ramsey, S. B. Leeb, T. DeNucci, J. Paris, M. Obar, R. Cox, C. Laughman, and T. J. McCoy, "Non-intrusive monitoring for condition-based maintenance," in *American Society of Naval Engineers Reconfigurability and Survivability Symposium*, Atlantic Beach, Florida, February 2005.

[4] S. B. Leeb, S. R. Shaw, and J. J. L. Kirtley, "Transient event detection in spectral envelope estimates for nonintrusive load monitoring," *IEEE Transactions on Power Delivery*, vol. 10, no. 3, pp. 1200–1210, July 1995.

[5] L. K. Norford and S. B. Leeb, "Non-intrusive electrical load monitoring in commercial buildings based on steady state and transient load-detection algorithms," *Energy and Buildings*, vol. 24, pp. 51–64, 1996.

[6] U. A. Khan, S. B. Leeb, and M. C. Lee, "A multiprocessor for transient event detection," *IEEE Transactions on Power Delivery*, vol. 12, no. 1, pp. 51–60, 1997.

[7] S. R. Shaw, S. B. Leeb, L. K. Norford, and R. W. Cox, "Nonintrusive load monitoring and diagnostics in power systems," *IEEE Transactions on Instrumentation and Measurement*, vol. 57, no. 7, pp. 1445–1454, July 2008.

[8] G. R. Mitchell, R. W. Cox, J. Paris, and S. B. Leeb, "Shipboard fluid system diagnostic indicators using non-intrusive load," *Naval Engineers Journal*, vol. 119, no. 1, November 2007.

[9] J. P. Mosman, R. W. Cox, D. McKay, S. B. Leeb, and T. McCoy, "Diagnostic indicators for shipboard cycling systems using non-intrusive load monitoring," in *American Society for Naval Engineers Day 2006*, Arlington, VA, June 2006.

[10] R. W. Cox, P. Bennett, D. McKay, J. Paris, and S. B. Leeb, "Using the non-intrusive load monitor for shipboard supervisory control," in *IEEE Electric Ship Technologies Symposium*, Arlington, VA, May 2007.

[11] G. Mitchell, R. W. Cox, M. Piber, P. Bennett, J. Paris, W. Wichakool, and S. B. Leeb, "Shipboard fluid system diagnostic indicators using nonintrusive load monitoring," in *American Society for Naval Engineers Day 2007*, Arlington, VA, June 2007.

[12] E. Proper, R. W. Cox, S. B. Leeb, K. Douglas, J. Paris, W. Wichakool, L. Foulks, R. Jones, P. Branch, A. Fuller, J. Leghorn, and G. Elkins, "Field demonstration of a real-time non-intrusive monitoring system for condition-based maintenance," in *Electric Ship Design Symposium*, National Harbor, Maryland, February 2009.

[13] G. Mitchell, "Shipboard fluid system diagnostics using non-intrusive load monitoring," Master's thesis, Massachusetts Institute of Technology, Department of Mechanical Engineering, June 2007.

[14] P. Bennett, "Using the non-intrusive load monitor for ship-board supervisory control," Master's thesis, Massachusetts Institute of Technology, Department of Mechanical Engineering, June 2007.

[15] M. Piber, "Improving shipboard maintenance practices using non-intrusive load monitoring," Master's thesis, Massachusetts Institute of Technology, Department of Mechanical Engineering, June 2007.

[16] E. Proper, "Automated classification of power signals," Master's thesis, Massachusetts Institute of Technology, Department of Mechanical Engineering, June 2008.

[17] R. Jones, "Improving shipboard applications of non-intrusive load monitoring," Master's thesis, Massachusetts Institute of Technology, Department of Mechanical Engineering, June 2008.

[18] A. Jones, "Harmonic approaches to non-intrusive load diagnostics," Master's thesis, Massachusetts Institute of Technology, Department of Mechanical Engineering, June 2008.

[19] P. Branch, "Development of real-time non-intrusive load monitor for shipboard fluid diagnostics," Master's thesis, Massachusetts Institute of Technology, Department of Mechanical Engineering, June 2008.

[20] T. DeNucci, "Diagnostic indicators for shipboard systems using non-intrusive load monitoring," Master's thesis, Massachusetts Institute of Technology, Department of Mechanical Engineering, June 2005.

[21] T. D. McKay, "Diagnostic indicators for shipboard mechanical systems using non-intrusive load monitoring," Master's thesis, Massachusetts Institute of Technology, Department of Mechanical Engineering, June 2006.

[22] Z. Clifford, Masters Thesis (unpublished), Massachusetts Institute of Technology, Department of Electrical Engineering and Computer Science, expected June 2009.

[23] S. R. Shaw, "System identification techniques and modeling for nonintrusive load diagnostics," PhD, Massachusetts Institute of Technology, Department of Electrical Engineering and Computer Science, February 2000.

[24] S. B. Leeb, "A conjoint pattern recognition approach to nonintrusive load monitoring," PhD, MIT, Department of Electrical Engineering and Computer Science, February 1993.

[25] C. R. Laughman, S. R. Shaw, S. B. Leeb, L. K. Norford, R. W. Cox, K. D. Lee, and P. Armstrong, "Power signature analysis," *IEEE Power and Energy Magazine*, pp. 56–63, March 2003.

[26] J. Paris, "A framework for non-intrusive load monitoring and diagnostics," Master's thesis, Massachusetts Institute of Technology, Department of Electrical Engineering and Computer Science, February 2006.

[27] S. R. Shaw and C. R. Laughman, "A kalman-filter spectral envelope preprocessor," *IEEE Transactions on Instrumentation and Measurement*, vol. 56, no. 5, pp. 2010–2017, October 2007.

[28] Z. Remscrim, Masters Thesis (unpublished), Massachusetts Institute of Technology, Department of Electrical Engineering and Computer Science, expected June 2010.

[29] E. W. Weisstein, "Mathworld," Available http://mathworld.wolfram.com/.